ARTICLES
PUBLISHED ONLINE: 18 SEPTEMBER 2017 | DOI: 10.1038/NPHYS4265
nature physics

Laser amplification in excited dielectrics

Thomas Winkler[1]*, Lasse Haahr-Lillevang[2], Cristian Sarpe[1], Bastian Zielinski[1], Nadine Götte[1], Arne Senftleben[1], Peter Balling[2]* and Thomas Baumert[1]*

Wide-bandgap dielectrics such as glasses or water are transparent at visible and infrared wavelengths. This changes when they are exposed to ultrashort and highly intense laser pulses. Different interaction mechanisms lead to the appearance of various transient nonlinear optical phenomena. Using these, the optical properties of dielectrics can be controlled from the transparent to the metal-like state. Here we expand this range by a yet unexplored mechanism in excited dielectrics: amplification. In a two-colour pump–probe experiment, we show that a 400 nm femtosecond laser pulse is coherently amplified inside an excited sapphire sample on a scale of a few micrometres. Simulations strongly support the proposed two-photon stimulated emission process, which is temporally and spatially controllable. Consequently, we expect applications in all fields that demand strongly localized amplification.

Focusing a femtosecond laser pulse on or inside transparent materials such as glasses or tissue leads to a well-defined deposition of energy by promoting a large density of carriers to the conduction band (CB). As this energy stays spatially confined on ultrashort timescales, these laser pulses have become the instrument of choice for dielectric structuring on a micrometre or even nanometre scale[1], as well as for applications in nanosurgery[2]. Depending on the incident intensity, a large range of material modifications can be realized: while the optical Kerr effect, self[3]- and cross-phase[4] modulation or field-induced currents[5] are examples of reversible processes, higher intensities can cause permanent refractive index changes[6,7], ablation of the material, or even the creation of new material phases[8]. A detailed overview of laser excitation in dielectrics can be found in Balling and Schou[9] and references therein.

The transient free-carrier density plays a fundamental role in determining the optical properties, and time-resolved 'pump–probe' experiments are excellent for studying its dynamics. Many experiments show that absorption and reflection increase after excitation due to the build-up of a transient electron plasma. This gives the material transient metallic properties that eventually prevent transmission through the dielectric material.

In contrast, this study provides the first demonstration of laser amplification in excited dielectrics (LADIE). For a certain intensity range of laser excitations with an 800 nm pump pulse, the dielectric material amplifies a time-delayed 400 nm probe pulse. This amplification starts to increase around 100 to 200 fs after excitation and is sustained for several tens of picoseconds; it is coherent in nature, and is present well below the visible ablation threshold of a thin sapphire sample (see cartoon of the process in the lower panel of Fig. 1). Supporting evidence, that LADIE may be a general feature of short-pulse-excited dielectrics, is also given: simulations, results for fused silica, and the relation to earlier unexpected high-transmission observations in water[10,11] are discussed in the article and the Supplementary Information.

Temporal dynamics in global and local amplification

The two-colour pump–probe scheme is sketched in Fig. 1. Figure 2a shows the global transmission of the probe pulse (blue squares) measured with a calibrated 3-eV-bandgap photodiode as a function of the pump–probe delay time. Negative times represent the case in which the probe pulse propagates through the unexcited sapphire sample, whereas for positive times it encounters the excited sample. For negative times no change in transmission is observed. As the delay time approaches zero, the global transmission of the 400 nm probe pulse increases to nearly two for a short time during the temporal overlap of pump and probe pulse. During the overlap, nonlinear interactions based on the optical Kerr effect[3] (OKE) cause cross-phase modulation[4] and parametric amplification[12]. Within 100–200 fs after the temporal overlap, the global transmission increases again up to 1.5, providing a direct experimental demonstration of a global gain for the probe pulse as it passes through the laser-excited sapphire.

This global behaviour is also reflected in the charge-coupled device (CCD) images of the probe pulse in Fig. 2b, where the images in addition show local contributions: in Fig. 2b(I) the unperturbed probe pulse after the sample is imaged, whereas in Fig. 2b(II) probe and pump pulses overlap temporally. 100 fs after the pump pulse (Fig. 2b(III)), the central part shows absorption, while for longer delay times a bright inner ring is observed (Fig. 2b(IV)). A Supplementary Movie is available for this scan. The movie shows the delay-time-dependent CCD images, overlaid with the global transmission of the probe pulse. Please note that the applied pump fluence of 2.7 J cm^{-2} is below the measured visible ablation threshold (3.2 J cm^{-2}) of sapphire. We define 'ablation' as the permanent material modification[13] visible in optical transmission microscopy.

The local transmission within the bright ring in Fig. 2b (IV) reaches a factor of 1.4. In the temporal evolution (red circles in Fig. 2c), this local transmission experiences a strong decrease during the overlap between pump and probe pulses, as reported in a manifold of studies[11,14–16]. Shortly after the pump pulse, the probe exhibits very low transmission followed by a slow increase. The maximum local amplification is reached at around 300 fs. Global (Supplementary Fig. 3) and local amplification is measurable up to delays of 50 ps.

To quantify the spatial features as a function of the pump–probe delay time, we take the difference between the excited and the unexcited sample along a horizontal line through the beam: Fig. 2d shows the difference signal versus the radial position r and

[1]Institute of Physics and CINSaT, University of Kassel, Heinrich-Plett-Strasse 40, D-34132 Kassel, Germany. [2]Department of Physics and Astronomy, Aarhus University, Ny Munkegade 120, DK-8000 Aarhus C, Denmark. *e-mail: winkler@physik.uni-kassel.de; balling@phys.au.dk; baumert@physik.uni-kassel.de

© 2017 Macmillan Publishers Limited, part of Springer Nature. All rights reserved.

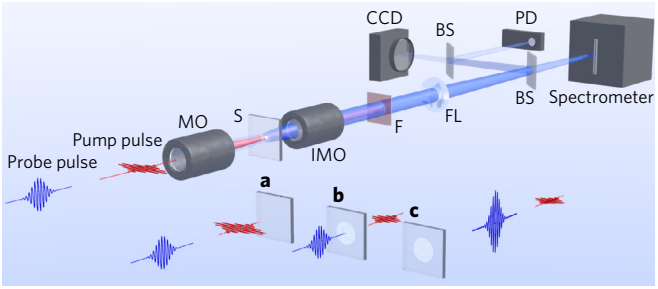

Figure 1 | Schematic of laser amplification in excited dielectrics (LADIE). Top: In-line pump–probe set-up. A horizontally polarized 800 nm bandwidth-limited femtosecond laser pulse with a pulse duration of 30 fs full-width at half-maximum (FWHM) excites a thin (131 μm) sapphire sample (ultraviolet-grade, C-plane), while a time-delayed vertically polarized 400 nm pulse (43 fs FWHM) is used to probe changes in the optical properties. The polarization of the probe pulse was chosen to provide highest reflectivity at the beamsplitters. The probe pulse is imaged by a 40× magnifying imaging system (20× IMO and 400 mm FL) onto a CCD camera, a 3-eV-bandgap photodiode and the entrance slit of an imaging spectrometer. The complete set-up is presented and discussed in detail in the Supplementary Information (Supplementary Fig. 1). The components are: MO—2× Focusing microscope objective, S—Sample, IMO—20× Imaging microscope objective, F—two 400 nm OD4 bandpass filters, FL—400 mm focusing lens, BS—(Pellicle-) beamsplitters, PD—calibrated 3 eV photodiode. Bottom: Snapshot of the LADIE process: before excitation (**a**), after strong-field excitation by the 800 nm pump pulse (**b**) and after the 400 nm probe pulse was amplified (**c**). The white shaded area in **b** and **c** indicates the excited state of the sample.

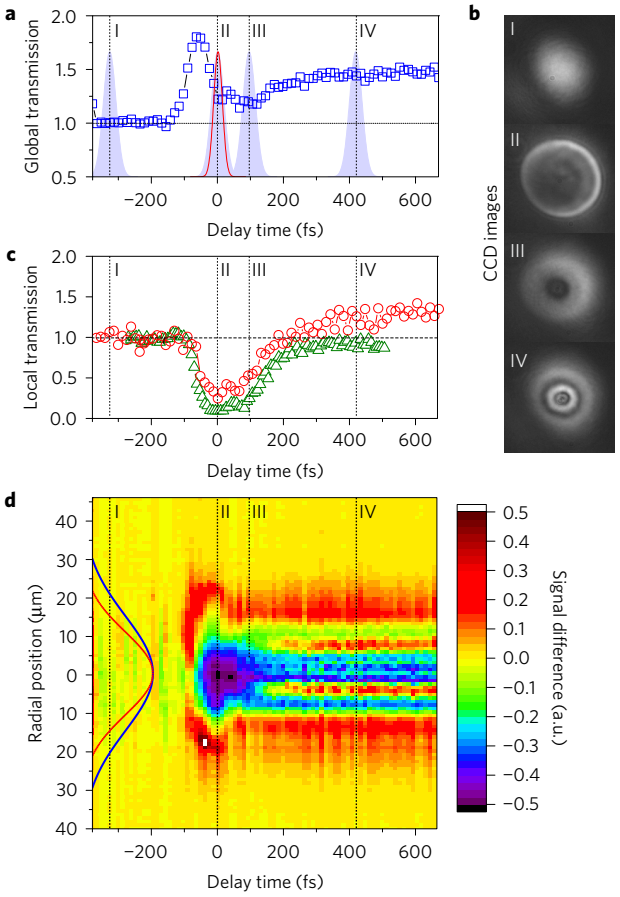

Figure 2 | Temporal dynamics of LADIE in excited sapphire. a, Spatially integrated transmission of the probe pulse. The red-solid Gaussian centred around time zero sketches the pump pulse (30 fs FWHM). The temporal delay between pump and probe pulse at certain values (Roman numbers) is visualized by blue-shaded Gaussians of 43 fs FWHM. **b**, CCD images of the probe pulse. Vertical dashed lines and Roman numbers in **a**,**c**,**d** represent the times at which CCD images in **b** were taken. **c**, Pump–probe-delay-time-dependent local transmission extracted at a radius of 5 μm to 7 μm from the CCD images (red circles) and measured by spectral interference (green triangles), extracted from Supplementary Fig. 5c. **d**, 2D difference plot of the cross-section of the CCD images for a pumped and an unexcited sample as a function of delay time. Red and blue lines represent the spatially Gaussian beam profiles of pump and probe beams. The experimental parameters were: probe-pulse peak fluence: 40×10^{-3} J cm^{-2}, pump-pulse peak fluence: 2.6 J cm^{-2}.

the pump–probe delay time. The spatial dimensions of the pump (red line) and probe pulses (blue line) are indicated by the Gaussians along the left axis. At time zero, we observe a negative difference at the centre ($r = 0$ μm) which is interpreted as absorption[11,17,18]. At large radii, the difference is positive, which is also seen as a bright outer ring in the CCD image (Fig. 2b(II)). This behaviour results from nonlinear propagation during the temporal overlap of the pulses.

At later times, the negative difference in the centre persists. This is attributed to free-carrier absorption by the CB electrons created by the pump pulse through strong-field excitation[14,15]. An overview of those mechanisms—that is, multiphoton and avalanche ionization—can be found in Balling and Schou[9]. The strong absorption is seen as a dark area in the centre of the probe pulse in Fig. 2b(III). In addition, a positive difference at larger radii remains. As these features are observed as soon as CB electrons are generated, we relate them to signatures of plasma scattering and defocusing of the probe pulse[19]. This effect might also contribute to a reduced transmission at positions of small radii. At longer delay times, two lines of positive difference located in the range of $r = 5$ μm to 7 μm appear, which are signatures of the local amplification seen as the bright inner ring in Fig. 2b(IV).

Figure 2c compares the temporal evolution of local transmission in this ring (red circles) to results of a spectral interference measurement (green triangles), which is sensitive only to coherent emission. Qualitatively, the dynamics are identical, confirming that the observed light amplification in dielectrics provides coherent radiation.

The specific spatial structure of the local amplification depends strongly on the applied pump fluence and can be directly extracted from Fig. 3a–c. A dependence on the spot sizes is discussed in the Supplementary Information.

Amplification dependence on the pump-pulse fluence

In Fig. 3a, CCD images of the probe pulse are shown for increasing pump-pulse peak fluence. We used a fixed pump–probe delay time of 500 fs, at which pump and probe pulses are clearly separated in time. At low pump fluence, we observe no changes in the beam profile of the probe pulse (Fig. 3a(i)). A higher value leads to absorption, seen as the black spot in Fig. 3a(ii). Increasing the pump fluence to 2.2 J cm^{-2} leads to the appearance of local amplification, seen as the bright spot in Fig. 3a(iii). Note that around the amplification area, absorption is still visible as a dark ring. Further increase of the pump fluence allows the amplification to move to larger radii, whereas in the centre the transmission decreases (Fig. 3a(iv)). As the amplification area follows the local fluence distribution of the pump pulse, we look now at the local dependencies.

In Fig. 3b,c, the radially resolved pump-fluence-dependent phase-shift and transmission values are shown. Note that all our measurements integrate along the propagation of the probe pulse through the excited sample. The data is obtained via spectral interference of the probe beam with a reference beam (see

© 2017 Macmillan Publishers Limited, part of Springer Nature. All rights reserved.

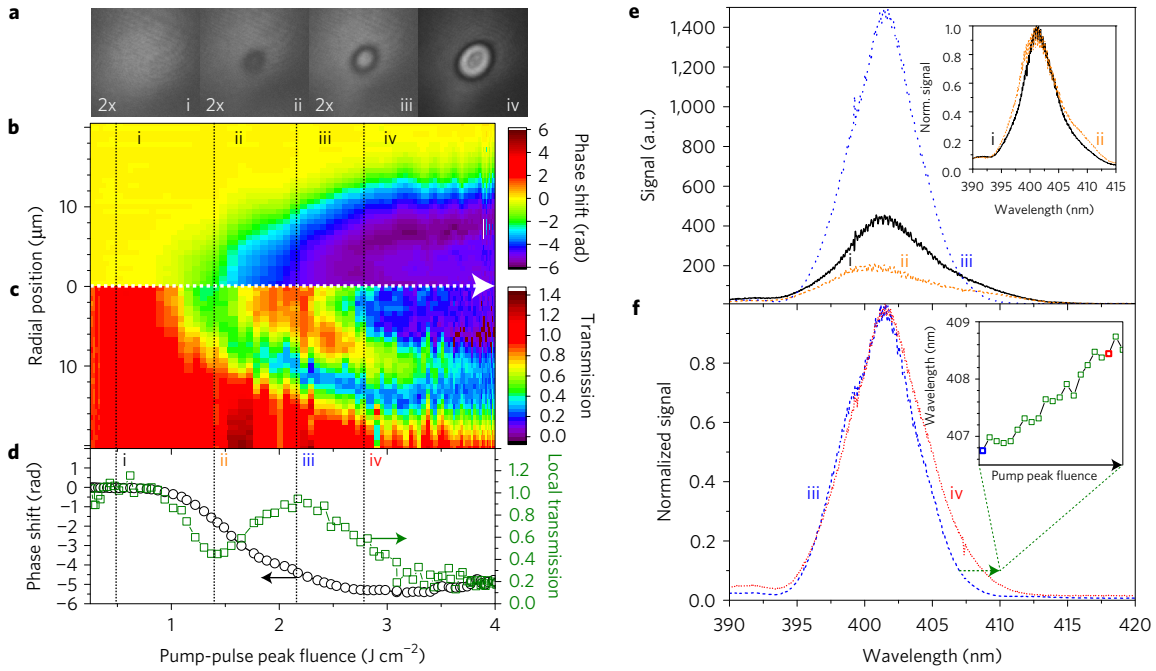

Figure 3 | Pump-fluence dependence of LADIE in sapphire 500 fs after excitation. a, Pump–probe CCD images extracted at pump fluences indicated by the vertical dotted lines in **b**–**d**. The 2× indicates that the brightness was doubled. **b**, Radially resolved phase shift. **c**, Radially resolved transmission. Phase shift and transmission were obtained by spectral-interference measurements. **d**, Phase shift (black circles) and transmission (green squares) extracted from the centre line in **b** and **c** (indicated by the white dashed arrow). **e**, Spectrum of the transmitted probe pulse extracted for different pump fluences, indicated by small Roman numbers (same as in **b**–**d**): i is the reference spectrum without excitation, ii is taken at absorption, iii at maximum amplification. The inset shows the normalized spectra for no excitation (i) and absorption (ii). **f**, Normalized spectra for maximum amplification and a higher probe fluence (iv). The inset in **f** represents the longest wavelength at which the normalized signal reaches 0.1 as function of the pump fluence (from 2 J cm^{-2} to 2.75 J cm^{-2}). The experimental parameters for **b**–**d** were probe-pulse peak fluence 15×10^{-3} J cm^{-2}. The experimental parameters for **a**,**e**,**f** were probe-pulse peak fluence: 50×10^{-3} J cm^{-2}. The reason for a lower probe-pulse fluence in spectral interference measurements is discussed in the Supplementary Information. Pump–probe delay time: 500 fs.

Supplementary Information), as this provides the most sensitive way of measuring the coherent changes in transmission. We used a probe-beam diameter, which exceeds the pump beam by more than 2.5 times[10,11], assuring that the local probe fluence is nearly constant over the excited area.

The phase shift represents the change in the real part of the refractive index during and after the excitation. An increase in the real part of the refractive index results in a positive phase shift, whereas a decrease leads to a negative phase shift, for example, caused by free electrons[11,15]. For low pump fluences, no change in the phase shift is visible. However, as soon as the threshold for strong-field excitation is reached at about 0.8 J cm^{-2}, an increase in fluence leads to a negative phase shift, as seen in Fig. 3b. The curve for the phase shift along the centre line (Fig. 3d) reaches its minimum of around −6 radians at a peak fluence of approximately 3 J cm^{-2}, close to the measured visible ablation threshold at 3.2 J cm^{-2} in our experiments. Higher pump fluences lead to a slightly increased (that is, less negative) phase shift, which has been observed for water[10,11] and sapphire[20] as well.

We observe that the phase-shift values follow the spatial pump-fluence distribution of a Gaussian beam up to the maximum change of the phase shift, as seen in Fig. 3b. For higher fluences, the radial distribution of the phase ceases to follow the local fluence. We expect self-induced propagation effects[21] of the pump pulse to be negligible below this threshold[11,22]. Note that the onset of amplification is observed well below this pump fluence.

The radially resolved transmission data in Fig. 3c show that regions of absorption and local amplification also follow the spatial pump-fluence distribution up to 3 J cm^{-2}, indicating that LADIE is linked to a certain local fluence, and thereby to a certain phase shift and excitation. Depending on the pump-pulse energy, the local amplification is either in the centre of the pump pulse, as shown in Fig. 3a(iii), or at higher radii, as a ring-like shape (Fig. 3a(iv)). In Fig. 3d, the local transmission in the centre of the pump pulse (green squares) is shown. It decreases with increasing pump fluence, as it was observed in a manifold of studies on laser-excited dielectrics[10,11] and is seen as the dark area in Fig. 3a(ii). However, at around 1.5 J cm^{-2} peak fluence, it starts to increase to nearly one again before it finally drops. We attribute this increase in transmission after initial absorption to LADIE.

Spectral properties of LADIE

The coherent nature of the measured local amplification in spectral interference is a strong indication for stimulated emission. In such a process, we expect spectral changes of the amplified light in addition. In Fig. 3e we present the measured spectra of probe pulses that propagated through samples that were unexcited (black solid line), excited to a strong absorption regime (orange dashed line), or excited to strong amplification (blue dotted line). The spectra were taken at a single radial position $r = 0\,\mu$m in the pump–probe configuration and at the fluences indicated in Fig. 3b–d by the lower Roman numbers (i–iv). In case of absorption (Fig. 3e(ii)), nearly all parts of the probe spectrum are absorbed; only in the wavelength regime above 413 nm is the absorption less strong. In the case of amplification (Fig. 3e(iii)) at higher pump fluence, we observe that the central wavelength of 402 nm is strongly amplified by almost a factor of 3.7 for the given experimental conditions.

The inset in Fig. 3e displays normalized spectra for the unexcited case (i) in comparison to strong absorption (ii). We observe a slight spectral broadening, especially in the red wing in case

© 2017 Macmillan Publishers Limited, part of Springer Nature. All rights reserved.

of absorption, which we attribute to an additional absorption process of nonlinear order. Additional evidence for this nonlinear absorption process is presented in detail in the Supplementary Information (Supplementary Fig. 7).

Figure 3f shows the normalized spectra in the case of maximum amplification (iii) and for a higher pump power (iv). With increasing pump fluence, the narrow amplification spectrum broadens towards longer wavelengths. The inset emphasizes this by showing the longest wavelength at a 10% level of spectral intensity as a function of the applied pump fluence. By increasing the peak fluence of the pump pulse from 2 to 2.75 J cm^{-2}, this long-wavelength limit increases by ∼2 nm. The amplified spectrum is significantly narrower than the spectrum in the case of no excitation, which points to a nonlinear amplification process.

Probe-pulse-fluence dependence of the amplification

To clarify the hints towards a nonlinear amplification process, we investigated the dependence of the transmission on the probe-pulse fluence. We used a fixed delay time of 500 fs and a pump fluence of 2 J cm^{-2}.

In terms of a spatially averaged, global transmission, we observe that at low probe-pulse fluence the transmission through the excited sample (red circles in Fig. 4a) is smaller than in the unexcited case (black squares), generally agreed upon in the literature as being caused by free-carrier absorption[15,18,20]. For a fluence above 0.16 J cm^{-2}, global gain can be obtained under the given experimental conditions, which is a strong indication that the amplification effect is not caused by light redistribution due to plasma defocusing[19] or diffraction. We again notice strong differences of local amplification (inner part) and local absorption (first black ring) seen in the image of the probe pulse in the right inset in Fig. 4a. As the global measurement is averaging over these features, we also investigated the local dependencies.

In Fig. 4b, the local probe-energy-dependent transmission of an amplified region (green diamonds), measured with the CCD camera, is shown. The position at which the data was evaluated is indicated by the inset in Fig. 4b. This data and the photodiode measurements (Fig. 4a) result from the same scan. As the CCD camera has a limited dynamic range, images only for probe energies above 0.18 μJ were recorded. We observe a nonlinear increase of the transmission with the incident probe-pulse energy and peak fluence, respectively. The increase of the local amplification with the probe peak fluence is clearly present in the spectral interference measurements (Supplementary Fig. 7) as well.

In the case of a lower pump-pulse excitation (see Fig. 3a), for which absorption is observed in the centre, the dependency on the probe-pulse fluence is different: the local transmission shows a slight decrease with increasing incident probe energy presented in the Supplementary Information (Supplementary Fig. 7), giving additional evidence of nonlinear absorption.

The nonlinear amplification process

The observed amplification in a bandgap material indicates that the conditions for stimulated emission are obtained. A simple two-level scheme would not allow those conditions to be fulfilled; therefore, a three-step amplification process is accounted for.

The first step towards the amplification is the excitation of sapphire by the IR pump pulse, leading to a non-equilibrium electron distribution in the CB, as sketched in Fig. 5a.

In the second step, the electronic system thermalizes due to electron–electron and hole–hole scattering. Usually within a hundred femtoseconds, after internal thermalization, the CB electrons and holes are in Fermi-like distributions[23], as shown in Fig. 5b.

In the final step, the probe pulse interrogates the excited dielectric, where the conditions for absorption or gain (by stimulated emission) depend on the difference of electron density in the CB

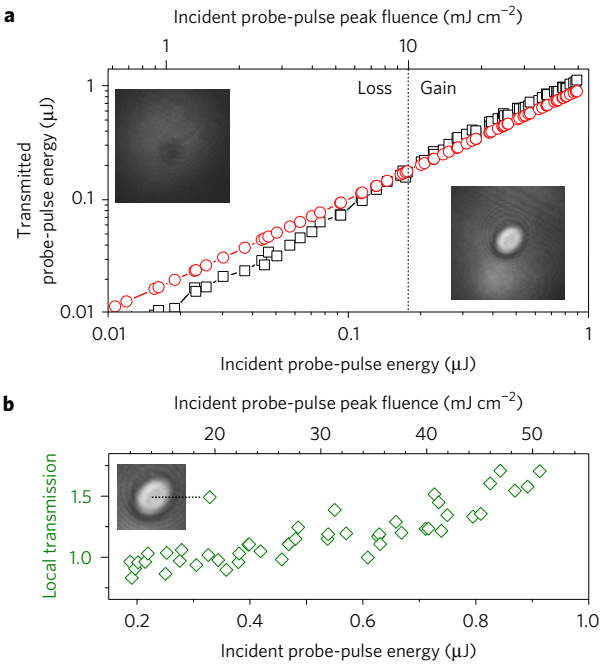

Figure 4 | Probe-fluence dependence of LADIE in excited sapphire 500 fs after excitation. a, Spatially integrated transmitted probe-pulse energy in a double-logarithmic representation for an unpumped (red circles) and excited sapphire sample (black squares). Insets in **a**: Exemplary CCD images of a transmitted probe pulse using very low (left) and very high probe-pulse energy after transmission. **b**, Green diamonds show the local transmission in dependence on the incident probe-pulse energy and fluence for an amplification region, as indicated on the inset. For convenience, the scale for the probe-pulse peak fluence is provided on the top axis of the graph. The experimental parameters were pump-pulse peak fluence 2 J cm^{-2} and pump–probe delay time: 500 fs.

and valence band (VB) at the transition energy ($E_T = n\hbar\omega_{Probe}$) (see details in the Supplementary Methods).

The order of a nonlinear absorption or stimulated process (n) is usually determined by the bandgap of the material. For ultraviolet-grade sapphire, a value of $E_{Gap} = 9.9$ eV (ref. 18) is typically measured. Therefore, the excitation of sapphire with 800 nm pulses is usually associated with a six- or seven-photon process[18,20,24].

To verify the proposed mechanism, we simulated the steps described above. The excitation of the sapphire sample is calculated via an extended multiple rate equation (MRE) model[25–27], which provides input for the quasi-Fermi distributions that describe the thermalized electrons and holes[23]. Finally, we use a simple propagation model taking into account free-carrier absorption, as well as nonlinear emission and absorption. The whole simulation is described in detail in the Supplementary Methods.

The red dashed line in Fig. 5c represents the simulated local depth-dependent transmission of the probe pulse, assuming a bandgap of sapphire at 9 eV, and therefore nonlinear stimulated emission or absorption for the 400 nm probe pulse of the third order. The transmission increases rapidly with increasing depth due to the self-reinforcing nature of multiphoton stimulated emission. However, at the depth where conditions for stimulated emission are no longer fulfilled (Supplementary Fig. 10), nonlinear absorption takes over, causing a dramatic decrease of the transmission, thus making it impossible for the initially amplified light to reach the end of the sample.

We thus propose that the main reason for a persistent amplification is carrier-induced bandgap shrinkage, as recently observed in bulk-silicon[28] and two-dimensional (2D) dielectric

© 2017 Macmillan Publishers Limited, part of Springer Nature. All rights reserved.

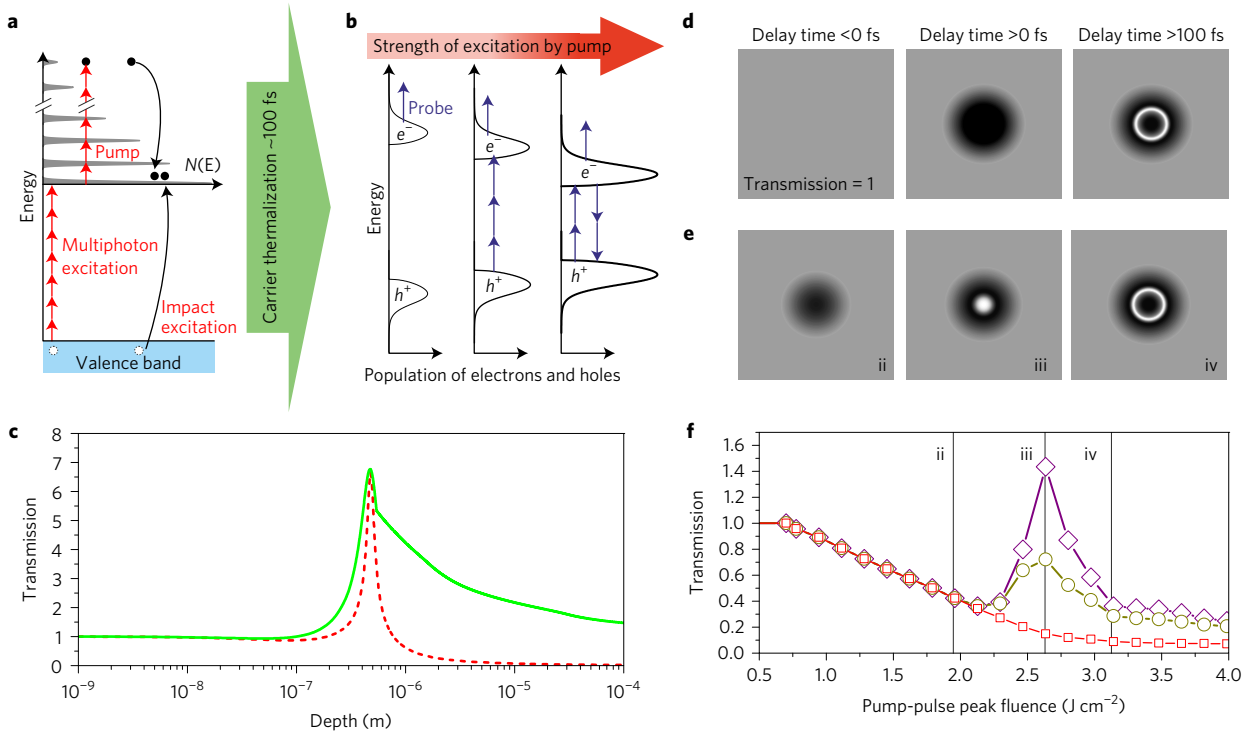

Figure 5 | Excitation and amplification mechanism and results of numerical simulations. a, Schematic drawing of the nonlinear excitation process by multiphoton absorption of the 800 nm pump pulse as well as impact excitation by high-energy electrons. The initial discrete electron distribution ($N(E)$) is sketched in the conduction band (shaded areas). **b**, Schematics of quasi-Fermi electron and hole distributions after carrier thermalization in dependence on the strength of excitation, indicating the carrier-dependent bandgap shrinkage as well. The blue arrows indicate free-carrier or nonlinear absorption or emission. **c**, Simulation of the depth-dependent transmission of the probe pulse (402 nm) in the case of a 9 eV bandgap and three-photon absorption/emission (red dashed line) and assuming a two-photon process based on bandgap shrinkage (to 6 eV) (green line). **d**, Simulated 'CCD' transmission images simulated before, shortly after excitation and after thermalization under amplification conditions (compare to Fig. 2b). **e**, Simulated transmission 'CCD' images for the indicated pump-pulse fluences (ii, iii, iv) in **f**. **f**, Simulation of temporally integrated local probe-pulse transmission for three different initial probe peak intensities, showing the dependency on the local pump-pulse fluence. The qualitative probe-pulse fluence is indicated by the size of the symbols (red squares ≪ yellow circles < purple diamonds). See corresponding experimental data in Fig. 3d.

materials[29,30]. When the sample is unexcited (red circles Fig. 4a), nonlinear absorption is not observed. Consequently, the probe pulse has insufficient intensity to induce multiphoton absorption processes. Only when the material is excited by at least 1 J cm^{-2}, spectral (Fig. 3) and transmission measurements (Supplementary Fig. 7) show signs of minor nonlinear ($n = 3$) absorption of the probe, indicating that the bandgap is effectively reduced to nearly 9 eV, starting at 9.9 eV, as indicated in Fig. 5b. A further increase of the pump fluence will presumably decrease the bandgap into the range of 6 eV and simultaneously transfer the material into a population-inversion state, allowing it to act as a two-photon gain medium for the probe light (see Supplementary Methods).

By taking into account the above-mentioned bandgap shrinkage in the propagation model, the gain achieved at the front of the material reaches the rear side (green line in Fig. 5c), and the simulation reproduces all main experimental observations:

Figure 5d shows simulated 'CCD' images of the probe-pulse transmission at different time steps: before and shortly after excitation, as well as after the electronic system has thermalized (>100 fs). The results are in excellent agreement with the experimental observations shown in Fig. 2b.

In Fig. 5e, simulated transmission 'CCD' images at three different pump-pulse fluences are shown, whereas Fig. 5f shows the simulated local pump-fluence-dependent transmission for three different probe-pulse fluences. The 'CCD' images as well as the local dependencies capture the main features, from the initial absorption to the amplification for a certain energy range as well as the local fluence dependency that leads to the appearance of a ring-like amplification structure, as was observed in the experiment (Fig. 3).

The applicability of LADIE to other dielectrics and a correlation of the effect to the presence of CB electrons was further elucidated by comparing the excitation of sapphire and fused silica, discussed in detail in the Supplementary Information (Supplementary Figs 4 and 5). In fused silica, LADIE is observed as well, but disappears rapidly after the excitation because the CB electron lifetime is dramatically reduced due to self-trapping[15]. Furthermore, in previous investigations of laser excitation in water[10,11], we observed an unexpectedly high transmission for a certain excitation strength, a phenomenon which we now attribute to LADIE.

As a final test of the proposed amplification process, we increased the excitation depth by utilizing temporally shaped pulses. In classical gain media, an increase of the gain length would result in a higher local amplification. Indeed, we observe a significant increase in local amplification due to an increase in excitation depth, shown and discussed in the Supplementary Information (Supplementary Fig. 8).

While temporal control of LADIE is given by the carrier-excitation and decay dynamics, spatial control on a micrometre and even smaller scale is possible via focusing and temporal pulse shaping, as recently demonstrated in the irreversible excitation regime[31]. The amplification effect may be maximized further by changing the excitation and amplification geometry from collinear to perpendicular. Therefore, we expect applications in all emerging fields that demand strongly localized amplification in time and space.

© 2017 Macmillan Publishers Limited, part of Springer Nature. All rights reserved.

Data availability. The data that support the plots within this paper and other findings of this study are available from the corresponding authors upon reasonable request.

Received 18 January 2017; accepted 17 August 2017; published online 18 September 2017

References

1. Gattass, R. R. & Mazur, E. Femtosecond laser micromachining in transparent materials. *Nat. Photon.* **2,** 219–225 (2008).
2. Chung, S. H. & Mazur, E. Surgical applications of femtosecond lasers. *J. Biophotonics* **2,** 557–572 (2009).
3. Shen, Y. R. Electrostriction, optical Kerr effect and self-focusing of laser beams. *Phys. Lett.* **20,** 378–380 (1966).
4. Islam, M. N., Simpson, J. R., Shang, H. T., Mollenauer, L. F. & Stolen, R. H. Cross-phase modulation in optical fibers. *Opt. Lett.* **12,** 625–627 (1987).
5. Schiffrin, A. *et al*. Optical-field-induced current in dielectrics. *Nature* **493,** 70–74 (2013).
6. Szameit, A. & Nolte, S. Discrete optics in femtosecond-laser-written photonic structures. *J. Phys. B: At. Mol. Opt. Phys.* **43,** 163001 (2010).
7. Mermillod-Blondin, A. *et al*. Time-resolved imaging of laser-induced refractive index changes in transparent media. *Rev. Sci. Instrum.* **82,** 33703 (2011).
8. Rapp, L. *et al*. Experimental evidence of new tetragonal polymorphs of silicon formed through ultrafast laser-induced confined microexplosion. *Nat. Commun.* **6,** 7555 (2015).
9. Balling, P. & Schou, J. Femtosecond-laser ablation dynamics of dielectrics: basics and applications for thin films. *Rep. Prog. Phys.* **76,** 36502 (2013).
10. Sarpe, C., Köhler, J., Winkler, T., Wollenhaupt, M. & Baumert, T. Real-time observation of transient electron density in water irradiated with tailored femtosecond laser pulses. *New J. Phys.* **14,** 75021 (2012).
11. Winkler, T. *et al*. Probing spatial properties of electronic excitation in water after interaction with temporally shaped femtosecond laser pulses. Experiments and simulations. *Appl. Surf. Sci.* **374,** 235–242 (2016).
12. Armstrong, J. A., Bloembergen, N., Ducuing, J. & Pershan, P. S. Interactions between light waves in a nonlinear dielectric. *Phys. Rev.* **127,** 1918–1939 (1962).
13. Mirza, I. *et al*. Ultrashort pulse laser ablation of dielectrics: thresholds, mechanisms, role of breakdown. *Sci. Rep.* **6,** 39133 (2016).
14. Haahr-Lillevang, L. *et al*. Short-pulse laser excitation of quartz. Experiments and modelling of transient optical properties and ablation. *Appl. Phys. A* **120,** 1221–1227 (2015).
15. Mao, S. S. *et al*. Dynamics of femtosecond laser interactions with dielectrics. *Appl. Phys. A* **79,** 1695–1709 (2004).
16. Temnov, V. V., Sokolowski-Tinten, K., Zhou, P. & von der Linde, D. Femtosecond time-resolved interferometric microscopy. *Appl. Phys. A* **78,** 483–489 (2004).
17. Garcia-Lechuga, M. *et al*. Simultaneous time-space resolved reflectivity and interferometric measurements of dielectrics excited with femtosecond laser pulses. *Phys. Rev. B* **95,** 214114 (2017).
18. Wædegaard, K. J., Sandkamm, D. B., Mouskeftaras, A., Guizard, S. & Balling, P. Probing ultrashort-pulse laser excitation of sapphire. From the initial carrier creation to material ablation. *Europhys. Lett.* **105,** 47001 (2014).
19. Gulley, J. R. & Dennis, W. M. Ultrashort-pulse propagation through free-carrier plasmas. *Phys. Rev. A* **81,** 33818 (2010).
20. Temnov, V. V., Sokolowski-Tinten, K., Zhou, P., El-Khamhawy, A. & von der Linde, D. Multiphoton ionization in dielectrics: comparison of circular and linear polarization. *Phys. Rev. Lett.* **97,** 237403 (2006).
21. del Hoyo, J. *et al*. Rapid assessment of nonlinear optical propagation effects in dielectrics. *Sci. Rep.* **5,** 7650 (2015).
22. Lanier, T. E. & Gulley, J. R. Nonlinear space-time focusing and filamentation of annular femtosecond pulses in dielectrics. *J. Opt. Soc. Am. B* **33,** 292–301 (2016).
23. Huthmacher, K., Molberg, A. K., Rethfeld, B. & Gulley, J. R. A split-step method to include electron–electron collisions via Monte Carlo in multiple rate equation simulations. *J. Comput. Phys.* **322,** 535–546 (2016).
24. Quéré, F., Guizard, S. & Martin, P. Time-resolved study of laser-induced breakdown in dielectrics. *Europhys. Lett.* **56,** 138–144 (2001).
25. Christensen, M. N., Byskov-Nielsen, J., Christensen, B. H. & Balling, P. Single-shot ablation of sapphire by ultrashort laser pulses. *Appl. Phys. A* **101,** 279–282 (2010).
26. Rethfeld, B. Unified model for the free-electron avalanche in laser-irradiated dielectrics. *Phys. Rev. Lett.* **92,** 187401 (2004).
27. Wædegaard, K., Sandkamm, D. B., Haahr-Lillevang, L., Bay, K. G. & Balling, P. Modeling short-pulse laser excitation of dielectric materials. *Appl. Phys. A* **117,** 7–12 (2014).
28. Schultze, M. *et al*. Attosecond band-gap dynamics in silicon. *Science* **346,** 1348–1352 (2014).
29. Johannsen, J. C. *et al*. Direct view of hot carrier dynamics in graphene. *Phys. Rev. Lett.* **111,** 27403 (2013).
30. Ebnonnasir, A., Narayanan, B., Kodambaka, S. & Ciobanu, C. V. Tunable MoS_2 bandgap in MoS_2–graphene heterostructures. *Appl. Phys. Lett.* **105,** 31603 (2014).
31. Götte, N. *et al*. Temporal Airy pulses for controlled high aspect ratio nanomachining of dielectrics. *Optica* **3,** 389–395 (2016).

Acknowledgements

The work was supported by the Otto-Braun-Funds, Deutsche Forschungsgemeinschaft (DFG) and the Danish Council for Independent Research | Natural Sciences. We highly acknowledge fruitful discussions with B. Rethfeld and her important input regarding our model.

Author contributions

The experiments were conceived and build by T.W., L.H.L., C.S. and B.Z. T.W. and L.H.L. carried out the experiments. T.W. and L.H.L. processed the data. L.H.L. and T.W. performed the simulations. Data were interpreted and discussed by all authors.

Additional information

Supplementary information is available in the online version of the paper. Reprints and permissions information is available online at www.nature.com/reprints. Publisher's note: Springer Nature remains neutral with regard to jurisdictional claims in published maps and institutional affiliations. Correspondence and requests for materials should be addressed to T.W., P.B. or T.B.

Competing financial interests

The authors declare no competing financial interests.

© 2017 Macmillan Publishers Limited, part of Springer Nature. All rights reserved.